# 8. Chapter 8: Preparation and evaluation $Ana_{C15:0}$ nanosponge based gel

## 8.1 Materials

**Table 8.1:** List of materials used in the study

| S.No | Materials | Source |
|---|---|---|
| 1. | HP-β-Cyclodextrin | Himedia Laboratories, Mumbai. |
| 2. | Carbonyldiimidazole | Himedia Laboratories, Mumbai. |
| 3. | Dimethylformamide | Himedia Laboratories, Mumbai. |
| 4. | HPMC K100M | Himedia Laboratories, Mumbai. |
| 5. | MMP-1 | Cell Signaling Technology, U.S.A. |
| 6. | HAT P300 | Cell Signaling Technology, U.S.A. |
| 7. | β-actin | Cell Signaling Technology, U.S.A. |
| All other chemicals were of analytical grade | | |

## 8.2 Methods

### *8.2.1 Analytical method*

#### *8.2.1.1 Calibration curve of Anacardic Acid ($Ana_{C15:0}$) in ethanol*

Stock solution (100 µg/mL) of $Ana_{C15:0}$ was prepared by dissolving 5 mg accurately weighed $Ana_{C15:0}$ in 50 mL ethanol. From the stock solution, 0.1, 0.2, 0.4, 0.6, 0.8, 1, 2 and 3 mL solutions were taken out using micropipette and diluted up to 10 mL with ethanol to finally obtain the concentrations of 1, 2, 4, 6, 8, 10, 20 and 30 µg/mL, respectively. These final solutions were analyzed using a UV-Visible spectrophotometer at 312 nm. Intra and interday precision was also determined.

#### *8.2.1.2 Calibration curve of $Ana_{C15:0}$ in phosphate buffer pH 6.8*

Stock solution (100 µg/mL) of $Ana_{C15:0}$ was prepared by dissolving 5 mg accurately weighed $Ana_{C15:0}$ in 50 mL ethanol. From the stock solution, 0.1, 0.5, 1, 2, 3, 4, and 5 mL

solutions were taken out using a micropipette and diluted up to 10 mL with phosphate buffer to finally obtain the concentrations of 1, 5, 10, 20, 30, 40 and 50 μg/mL respectively. These final solutions were analyzed using a UV-Visible spectrophotometer at 312 nm. Intra and interday precision was also determined.

### *8.2.2 Synthesis of β-Cyclodextrin Nanosponge*

β-Cyclodextrin nanosponge was synthesized as per the method described by Dora et al. 2016 (Dora, Trotta et al. 2016). Briefly, 13.75 g of anhydrous β-Cyclodextrin (10 mM) was dissolved in 100 mL dimethylformamide (DMF) in a round bottom flask under constant stirring till the formation of a clear solution. Further, 9.95 g of cross-linker carbonyldiimidazole (CDI; 40 mM) was added in the same flask and kept the reaction at 100°C for 24 h under magnetic stirring. After 24 h, the product was left to cool at room temperature, added an excess of double-distilled water, filtered, purified by soxhlet extraction with ethanol, which was further dried in vacuum and grounded in mechanical milling. Anhydrous β -CD, and CDI were taken in 1:4 molar ratios.

### *8.2.3 Preparation of $Ana_{C15:0}$ loaded Nanosponge complex*

Anacardic Acid nanosponge complex ($Ana_{C15:0}$-NS) was prepared by a previously established lyophilization method. Accurately weighed quantities of NS were suspended in 20 mL of HPLC grade water placed on a magnetic stirrer, followed by addition of $Ana_{C15:0}$ in a w/w ratio of 1:2, 1:3, and 1:4 ($Ana_{C15:0}$: nanosponge). Further, this mixture was sonicated for 10 min and kept for 24 h under stirring. The suspension was centrifuged at 4000 rpm for 10 min to separate the uncomplexed drug and the supernatant was lyophilized further (Labcono, U.S.A.). The condenser temperature was maintained at -60°C and pressure at 200 mT to obtain drug-loaded NS formulation. Mannitol (5 w/v %) was used as a cryoprotectant (Lembo, Swaminathan et al. 2013).

### *8.2.4 Optimization of $Ana_{C15:0}$-NS formulation using 3-level factorial design*

Optimization of formulation variables and their levels in $Ana_{C15:0}$-NS development was performed using 3 –level factorial design. The design was produced using Design Expert® 7.0 software for optimization of a two-component system. Formulation design involved two independent variables $Ana_{C15:0}$: NS ratio (X1) and sonication time (X2) with three levels (low, medium, and high). Particle size (Y1) and percentage entrapment efficacy (E.E. %) (Y2) were opted as dependent variables. All three mentioned dependent variables were considered as response parameters due to their crucial role in formulation desirability and performance (Pandya, Jani et al. 2018). The Design Expert 7.0 software designed a total of 13 experiments with 5 centre points, and the impact of varying independent variables on dependent variables (response parameters) was predicted utilizing response surface plots.

### *8.2.5 Evaluation of $Ana_{C15:0}$-Nanosponge*

#### *8.2.5.1 Determination of Particle size, Polydispersity index, and Zeta potential*

Particle size (PS), polydispersity index (PDI.), and zeta potential (ZP) of formulation were measured by photon correlation spectroscopy using Delsa Nano (Beckman coulter, U.S.A.). The samples were suitably diluted with HPLC grade water before every measurement (Zainuddin, Zaheer et al. 2017).

#### *8.2.5.2 Percentage entrapment efficiency (EE%)*

Entrapment efficiency was determined by the indirect method. The nanoparticle dispersion was centrifuged at 15,000 rpm in a cooling centrifuge (REMI, India, Model C-24) at 4 °C for 30 min. The supernatant was diluted suitably with ethanol, and the amount of $Ana_{C15:0}$ was determined by UV spectrophotometer (UV-1700 PharmSpec, Shimadzu) at a wavelength (λ) of 312 nm (Shringirishi, Mahor et al. 2017).

Percentage entrapment efficiency (EE%) was calculated from Equation (1) as follows:

**Equation (1):**

$$\text{EE\%} = \frac{\text{Total amount of drug(mg)} - \text{Free drug (mg)}}{\text{Total amount of drug (mg)}} \times 100$$

### *8.2.5.3 Solubility study*

The solubility of $Ana_{C15:0}$ and $Ana_{C15:0}$-NS (obtained from different ratios of drug and NS) was determined by shake flask method. Briefly, excess of $Ana_{C15:0}$ and $Ana_{C15:0}$-NS were added to HPLC grade water in sealed glass containers at 25°C. The samples were agitated at 100 rpm for 24 h in the shaker water bath then centrifuged at 10,000 rpm for 10 min. The supernatants were filtered (0.45 µm PVDF syringe filter, Millipore Millex-HV). The filtrate was suitably diluted with methanol and analyzed by a UV spectrophotometer (UV-1700 PharmSpec, Shimadzu) at 312 nm (Mihailiasa, Caldera et al. 2016).

### *8.2.5.4 Fourier transform infrared spectroscopy (FT-IR)*

The FT-IR spectra of $Ana_{C15:0}$, HP-β-CD, and $Ana_{C15:0}$-NS were recorded using a Fourier transform infrared spectrometer, Bruker Alpha II FTIR Spectrometer (Bruker Corporation, Germany). The samples were scanned at a spectral range of 500-400 cm-1 with a resolution of 2 cm-1 and 128 scans for each run. The samples were first diluted with KBr powder and compressed to form pellets for performing the measurements (Allahyari, Valizadeh et al. 2020).

### *8.2.5.5 X-ray diffraction (XRD) study*

The powder X-ray diffraction patterns of the pure compound $Ana_{C15:0}$, 2-HP-β-CD, $Ana_{C15:0}$-NS were examined by Rigaku Miniflex 600 Desktop X-Ray Diffraction system (Rigaku Corporation, Japan) using HyPix-400 MF 2D hybrid pixel array detector (HPAD). The current and voltage applied were 40 mA and 40 kV, respectively. The data

were recorded in the range of 2θ: 5–40 with scan rate 10°/min and step size 0.03° (Rafati, Zarrabi et al. 2019).

#### *8.2.5.6 Morphology evaluation of $Ana_{C15:0}$ encapsulated nanosponge*

The surface morphology of $Ana_{C15:0}$ encapsulated nanosponge was evaluated using Transmission Electron Microscope (Tecnai G2 20 TWIN, F.E.I. Company of U.S.A.). Approximately 3-4 drops of NS suspension were placed on a copper stub and air-dried later, sputter-coated with gold. Samples were analyzed at 3 kV accelerating voltage at a working distance of 200 mm (Clemente, Argenziano et al. 2019).

#### *8.2.5.7 In-vitro release study*

Dialysis bag diffusion method was employed to evaluate the *in-vitro* drug release pattern of $Ana_{C15:0}$-suspension and $Ana_{C15:0}$-NS. The dialysis bag (MCWO: 12-14 K.D.A.) was suspended in a glass beaker having 100 mL phosphate buffer (PBS) pH 6.8 containing 0.1% w/v SLS (solubility of the drug is very poor and hence 0.1% w/v S.L.S. was added to the buffer to maintain the sink condition as well to increase the solubility of the drug in the buffer). The beaker was placed on a magnetic stirrer with stirring speed 100 rpm, and temperature 37±0.5°C. Aliquots (1 mL) were withdrawn at predetermined time intervals (0.25, 0.5, 0.75, 1, 2, 3, 4, 8, 12 and 24 h) from the receptor compartment and replaced with fresh media. The samples were further diluted and analyzed using a UV-Vis spectrophotometer (Mognetti, Barberis et al. 2012).

### *8.2.6 Preparation of $Ana_{C15:0}$-NS enriched topical gel*

The gel base was prepared by using HPMC K100M as a gelling agent. Accurately weighed HPMC K100M was taken and dispersed slowly in a beaker containing distilled water with constant stirring using a mechanical stirrer at 500 rpm for 30 min. $Ana_{C15:0}$ and $Ana_{C15:0}$-NS were dispersed in the gel base under stirring to yield respective gels.

Methylparaben (0.3% w/v) was used as a preservative in the gel formulation (Butani, Yewale et al. 2016).

### *8.2.7 Evaluation of $Ana_{C15:0}$-NS topical gel*

#### *8.2.7.1 Texture profile analysis*

The characteristics of $Ana_{C15:0}$-NS topical hydrogel were assessed for changes in the properties like hardness, adhesiveness, and elasticity. These changes were examined using texture profile analysis (TX-XT Plus texture profile analyzer, Stable Micro Systems, U.K.). The system was set as TPA mode in which the probe was compressed in every sample at a definite rate (1 mm/s) to the depth of 15 mm along with a trigger force of 5 g (Gade, Patel et al. 2019).

#### *8.2.7.2 Ex-vivo skin permeation and retention study*

Female Albino Wistar rats weighing 200 ± 25 g were selected for the study. Hairs of abdominal skin were removed using a trimmer, and then the skin was excised and further checked for uniformity and integrity using a lamp-inspecting method. The excised skin was then rinsed with physiological saline, and fat tissues below the skin were chopped carefully. The uniform thickness of each skin was selected for the experiment. The processed skin samples were further placed between the donor and the receptor compartment of Franz diffusion cells. The effective diffusion surface area was 1.54 $cm^{2,}$ and a cell volume of 20 mL was used in the study. The receptor compartments were filled with freshly prepared mixtures of physiological buffer solution pH 6.8 containing 0.1% SLS which was used to solubilize the $Ana_{C15:0}$ and to maintain sink conditions. The temperature of Franz diffusion cells was maintained at 37 ± 0.5°C, and the fluid in the receptor chambers was stirred continuously at 300 rpm. The gels weighing 0.5 g were applied on the skin fixed towards the donor compartment and the aliquots (0.5 mL) were withdrawn at predetermined time intervals 0, 1, 2, 3, 4, 5, 6, 12 and 24 h and analyzed

using UV spectrophotometer at 312 nm (Gade, Patel et al. 2019). The equivalent volume of physiological buffer solution (pH 6.8) containing 0.1% SLS was replaced at every sampling point. The cumulative amounts of $Ana_{C15:0}$ permeated through the skin were plotted as a function of time. At the end of the experiments, the skins were removed and washed with distilled water. Further, skins were soaked in 5 ml of methanol for 24 h and were sonicated for 15 min each in a bath sonicato followed by separation via centrifugation. The amount of drug accumulated in the skin, i.e., the total amount of $Ana_{C15:0}$ extracted from the skin at the end of the skin permeation study (at 24 h), could be obtained from the concentration of $Ana_{C15:0}$ in supernatant methanol.

### *8.2.8 Animal Study*

Thirty female Wistar rats (150-200 gm) were selected for the study. The whole experiment was performed as per the procedure approved by the animal ethics committee of the Institute of Medical Sciences (Banaras Hindu University) Varanasi, India (Reference No: Dean/2017/CAEC/89). The rats were quarantined for seven days and evaluated for weight change and any sign of injury before the study begins. The animals were housed in plastic cages (three animals in each cage) with sawdust and kept in a 12/12 h light-dark cycle at a temperature of 25 ± 2°C. They were given a standard diet and water ad libetum. The animals were divided into five different groups, each containing six animals. Initially, the dorsal region of rats was depilated using a depilatory cream. Handheld PUVA (UV-B, 311 nm narrowband, 9 Watt), (Philips HP-602) lamp was used as a UV radiation source. The bulb was fixed in a UV chamber, and rats were kept in a restrainer to restrict their mobility while exposed to UV radiation (Feliciano and Nagasaki 2017). The positive control (group I) was not exposed to UV radiation. The negative control (group II: UV-B irradiated group) was exposed to UV radiation, but it was not given any treatment. The animals in group III, group IV, group V were exposed

to UV radiation, and then they were treated with blank gel, 0.1% w/w $Ana_{C15:0}$-gel, and 0.1% w/w $Ana_{C15:0}$-NS gel, respectively. Initially, for two weeks, animals were exposed to UV-B radiation for 10 min per day, then next one week for 15 min per day, and then in the last one week, they were exposed for 20 min per day.

#### *8.2.8.1 Histopathology study*

In order to perform a histopathological study, the dorsal skin of the rats was harvested, and then the skin samples were placed in 10% neutral buffered formalin for 1-2 days, embedded in paraffin, and cut into 5 mm thick sections. The sections were then stained with hematoxylin and eosin (H&E), examined, and photographed under a bright field microscope (Keyence BZ-X700) (Feliciano and Nagasaki 2017).

#### *8.2.8.2 Estimation of biochemical parameters*

##### *8.2.8.2.1 Determination of reactive oxygen species (ROS) level*

ROS production in the skin was examined using ROS indicator 2, 7 -dichlorodihydro-fluorescein (DCF) as reported earlier (Zhu, Li et al. 2017). The method involves two steps as described below:

***Sample preparation:*** The tissue samples were first cleaned and washed with buffer (working solution) to remove the fiber, fat, and other debris. The samples were then cut into small pieces (1 $mm^2$) and put into a working solution. Further, an appropriate amount of enzyme digestion (0.25% trypsin) was added and incubated at 37℃ in a water bath for 20~30 min and gently oscillated the mixture intermittently. The samples were filtered using a nylon mesh (300 mesh) to remove the massive components, and the cells were collected. The cells were further suspended in a working solution.

***Addition of DCF and detection***

The test samples (100 µL) were put into the different wells of a microplate reader (96 well plate), and then 10 µM of DCF were added to various wells containing test samples.

Relative amounts of ROS production were determined using a fluorometric plate reader (excitation 485 nm, emission 528 nm) (Bravo, Duque et al. 2017).

*8.2.8.2.2 Western blot study*

For western blot analysis, skin regions were lysed using a complete protease inhibitor cocktail, and concentration of protein was estimated as reported earlier (Bradford 1976). A standard curve was also plotted using bovine serum albumin. An equal amount of sample protein lysate (50 µg) as obtained from the sample treatment was subjected to 10% sodium dodecyl sulfate-polyacrylamide gel electrophoresis-polyacrylamide gel electrophoresis (SDS-PAGE) (Bio-Rad, Mini-PROTEAN® Tetra Cell). The bands were further isolated from the gel and transferred into a polyvinylidene-fluoride (PVDF) membrane employing electro-blotting. Furthermore, the membrane was blocked using 5% skim milk and then incubated with primary antibodies against MMP-1 (1:500, Cell Signaling Technology, U.S.A.) and HAT P300 (1:2000 Cell Signaling Technology, U.S.A.). All the bands were then visualized utilizing HRP-linked secondary antibodies (1:1000, Cell Signaling Technology, U.S.A.) employing Bio-Rad Gel Doc ® E.Z. Imager system. The image data analysis was performed using NIH Image J software (Cho, Bahuguna et al. 2017). All the western blot experiments were performed in triplicate, and data is presented as mean± standard deviation.

## 8.3 Results and Discussion

Poor aqueous solubility of drugs always remains a huge challenge for developing formulations. In the present study, we synthesized and characterized nanosponge based on the reaction between β-cyclodextrin monomer and CDI cross-linker. Furthermore, the nanosponge was utilized to prepare its complex with $Ana_{C15:0}$ with an aim to enhance its solubility and thus its bioavailability.

### *8.3.1 Analytical method*

A calibration curve (Figure 8.1) was prepared to calculate the $Ana_{C15:0}$ concentrations in the test samples while performing studies like solubility assay, determination of entrapment efficiency and in vitro release. The calibration of $Ana_{C15:0}$ was successfully prepared in ethanol and phosphate buffer pH 6.8 with linearity value ($R^2$) 0.9992 and 0.9991, respectively.

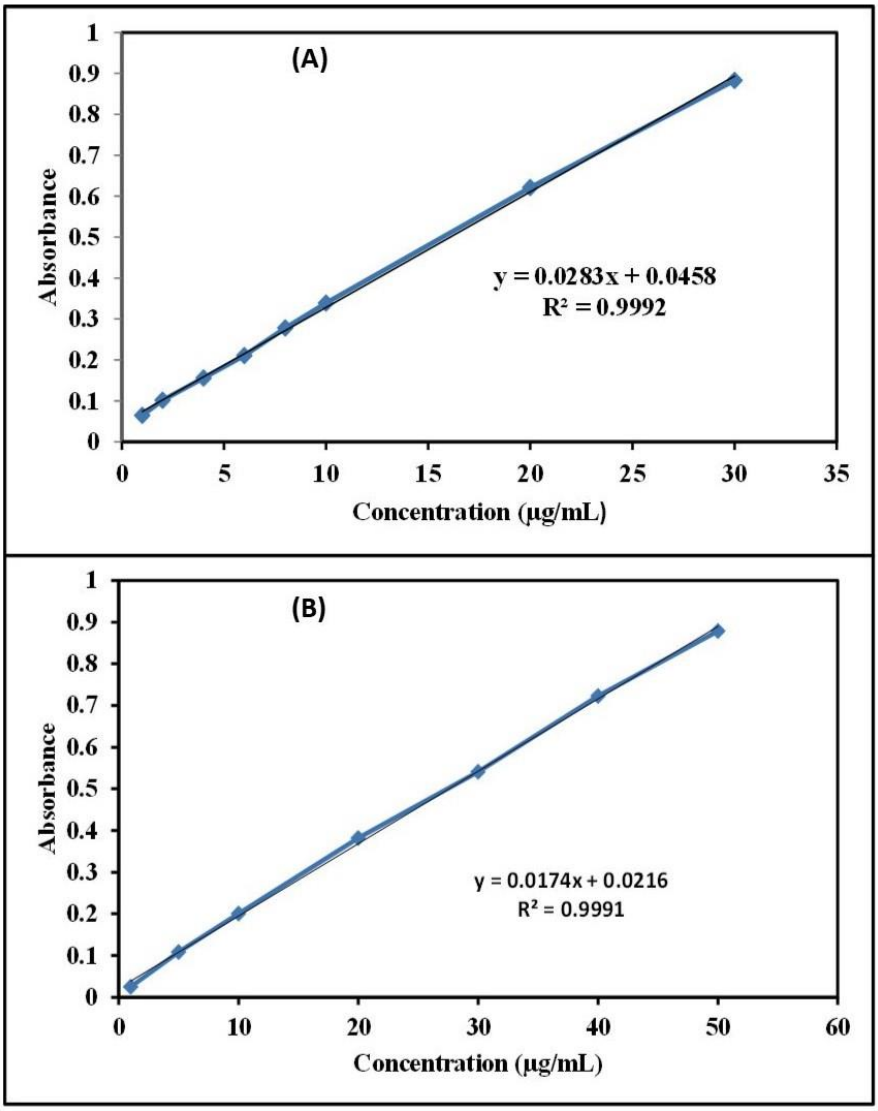


**Figure 8.1:** Calibration curve of $Ana_{C15:0}$ in ethanol (A), and phosphate buffer pH 6.8 (B) by using UV spectrophotometry. The graph indicates the absorbance at Y axis in response to the different concentrations on X axis.

### *8.3.2 Formulation optimization*

Design Expert was used for the formulation optimization. The optimization was carried out for process and formulation variables by a 3-level factorial design. Independent variables, $Ana_{C15:0}$: NS ratio and sonication time (min) were selected based on their effect on response parameters, particle size, and percentage entrapment efficiency (EE%).

**Table 8.2**: Experimental design demonstrating PS and EE% of the different formulation batches

| Run | Factor 1 A:Ana:NS ratio | Factor 2 B:Sonication Time (min) | Response 1 Particle Size (nm) | Response 2 Entrapment Efficiency (%) |
|---|---|---|---|---|
| 1 | 1:2 | 12.50 | 179.3 | 65.9 |
| 2 | 1:4 | 15.0 | 202.7 | 78.7 |
| 3 | 1:3 | 12.50 | 190.8 | 69.9 |
| 4 | 1:3 | 12.50 | 194.1 | 70.4 |
| 5 | 1:3 | 10.0 | 197.4 | 71.6 |
| 6 | 1:4 | 12.50 | 207.8 | 76.3 |
| 7 | 1:3 | 15.0 | 188.3 | 69.4 |
| 8 | 1:2 | 15.0 | 176.5 | 64.8 |
| 9 | 1:3 | 12.50 | 193.7 | 69.8 |
| 10 | 1:2 | 10.0 | 185.4 | 67.2 |
| 11 | 1:3 | 12.50 | 191.9 | 70.9 |
| 12 | 1:3 | 12.50 | 194.2 | 71.2 |
| 13 | 1:4 | 10.0 | 210.5 | 73.8 |

The layout of design variables, along with values of formulation parameters, is given in Table 8.2. Optimization of formulation batches was done by considering Particle size (Y1) and EE% (Y2). Response for each experiment was measured, and their quadratic model was fitted to carry out multiple regression analysis and F-statistic. A mathematical model was carried out to obtain a polynomial equation. The quadratic model was selected as the best suitable model. Polynomial equations for both particle size and EE% were obtained.

**The equation for particle size is given below;**

**Equation 2:**

$$\text{Particle Size} = +192.77 + 13.17 \times \text{A} - 4.33 \times \text{B}$$

From the above **Equation 2** and 3D response surface plot in Figure 8.2-A, it can be concluded that $Ana_{C15:0}$: NS ratio (Factor A) had a positive effect on particle size, i.e. particle size of NS increases with an increase in the $Ana_{C15:0}$: NS ratio and vice versa. In the case of sonication time (Factor B), it can be observed that particle size decreases with an increase in sonication time and vice versa.

**The equation for EE% is given as follows:**

**Equation 3:**

$$\text{EE\%} = +70.76 + 5.15 \times \text{A} + 0.050 \times \text{B} + 1.83 \times \text{A} \times \text{B}$$

From the above **Equation 3** and 3D response surface plot in Figure 8.2-B, it can be observed that factor A had a positive effect on EE% and hence with an increase in the $Ana_{C15:0}$: NS ratio, EE% increases, and vice versa. On the other hand, factor B did not show a significant effect on EE%.

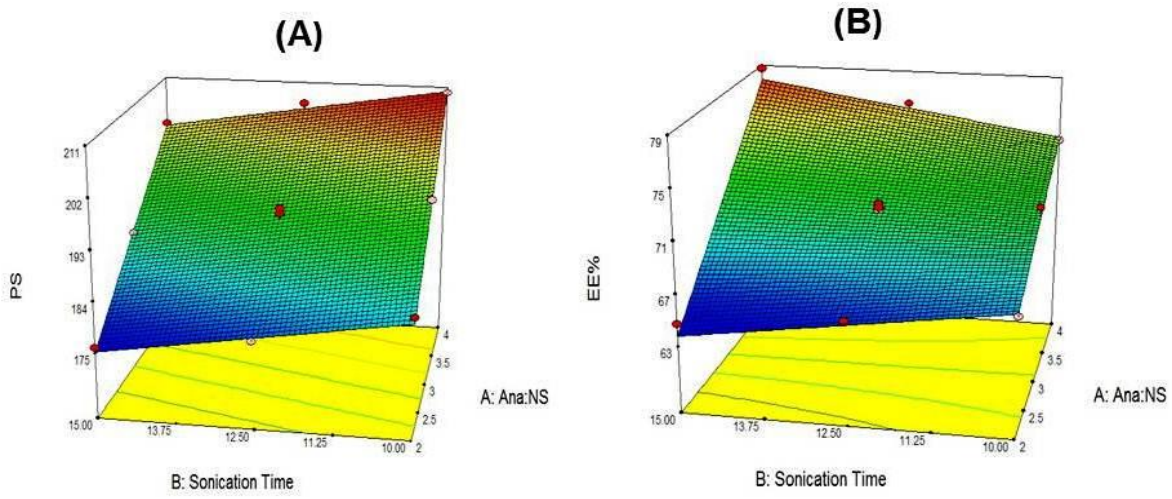


**Figure 8.2:** 3D plots indicating the effect of different formulation variables on PS (A) and EE% (B).

Further, based on the optimization results, the values of predicted formulation variables and their dependent variables were obtained from the design software. Furthermore, the optimized batch was prepared as per the suggested composition (Table 8.3), and the results of the predicted and experimental responses were compared. The data demonstrated in Table 8.4 indicates no significant difference between experimental and predicted responses.

**Table 8.3**: Identified independent variables with their levels used in 3-level factorial experimental design and the optimized levels of the variables

| **Code** | **Independent variables** | **Levels** | | | **Software Optimized level** |
|---|---|---|---|---|---|
| | | **Low** | **Medium** | **High** | |
| A | $Ana_{C15:0}$: NS ratio | 1:2 | 1:3 | 1:4 | 1:3.20 |
| B | Sonication time (min) | 10.0 | 12.5 | 15.0 | 13.90 |

**Table 8.4:** Predicted values of PS and EE% based on the optimized level and the experimental response obtained

| S. No. | Dependent variables | Predicted response | Experimental response |
|---|---|---|---|
| 1 | Particle size (nm) | 192.98 | 197.4±11.6 |
| 2 | Entrapment efficiency (%) | 72.04 | 74.8±2.9 |
| 3 | PDI | - | 0.276±0.028 |
| 4 | Zeta Potential (mV) | - | -22.1±1.9 |

### *8.3.3 Solubility study*

The solubility study of $Ana_{C15:0}$ and $Ana_{C15:0}$-NS in purified water with different w/w ratios of drug and nanosponge were evaluated. The solubility of all the nanosponge complexes was significantly higher ($p<0.001$) than pure $Ana_{C15:0}$ (5.48 ± 1.84 µg/mL). The solubility of $Ana_{C15:0}$ was optimum in 1:3 w/w proportions of drug and NS (32.20±2.98 µg/mL). Further, increase in drug and NS ratio did not enhance the solubility significantly, probably due to saturation solubility of the drug in NS. Therefore, we opted formulation with a 1:3 w/w ratio for further studies. The observed increase in solubility could be due to the inclusion of the drug within the lipophilic sites present within the nanosponge network.

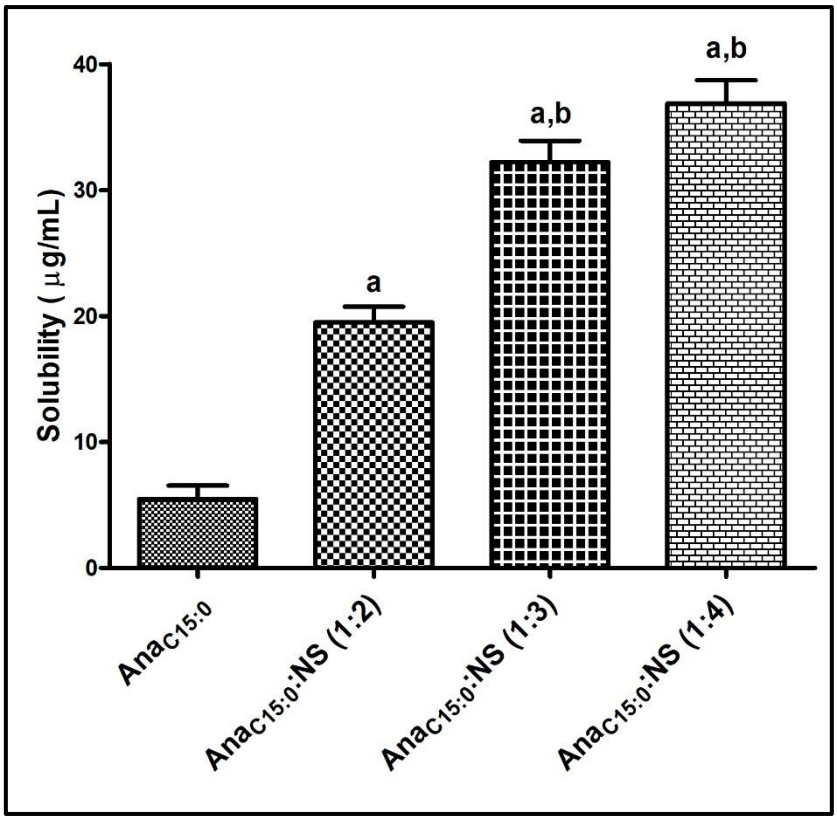


**Figure 8.3:** Comparative solubility profiles of $Ana_{C15:0}$ and different ratios of $Ana_{C15:0}$:NS. All experiments were performed in triplicate and data represented as mean±S.D (n=3). [a]represents significant difference as compared to $Ana_{C15:0}$, [a,b]represents significant difference compared to $Ana_{C15:0}$-NS (1:2). P<0.005, one-way ANOVA followed by Newman-Keuls multiple-comparison test.

### *8.3.4 Fourier transform infrared spectroscopy*

Formation of complexes, especially nanosponge complexes of drugs with cyclodextrins, can be widely assessed using FT-IR spectroscopy. This technique helps in determining the change in the bands of vibrations of compounds and cyclodextrins in the process of complex formation. Nanosponge formation is generally indicated by a change in intensity, disappearance, and widening as well as shifting of peaks. The FT-IR spectra of $Ana_{C15:0}$, HP-β-CD, nanosponge are shown in Figure 8.4. The FT-IR spectra of HP-β-CD (Figure 8.4) showed the presence of peaks at 3600–3000 $cm^{-1}$ (O-H stretching vibration), 1038 $cm^{-1}$ (C=O stretching vibration), and 2917 $cm^{-1}$ (C-H stretching vibrations). The

FT-IR spectra of $Ana_{C15:0}$ revealed the presence of all characteristic fingerprint peaks at 3420 and 1304 $cm^{-1}$ (Ar-OH), 3400-2400, 1645 $cm^{-1}$ and 1304 $cm^{-1}$ (-COOH), 3009 $cm^{-1}$ (Ar-H and vinyl-H), 2924 and 2849 cm-1 (aliphatic C-H), 1607 $cm^{-1}$ (aliphatic C=C), and 1446 $cm^{-1}$ (aromatic C=C). The nanosponge revealed distinct FT-IR spectra with the absence of absorption peaks at 2400-3400 $cm^{-1}$. The loss of aromatic peaks of $Ana_{C15:0}$ in the nanosponge could be an indication of entrapment of $Ana_{C15:0}$ inside the HP-β-CD cavity.

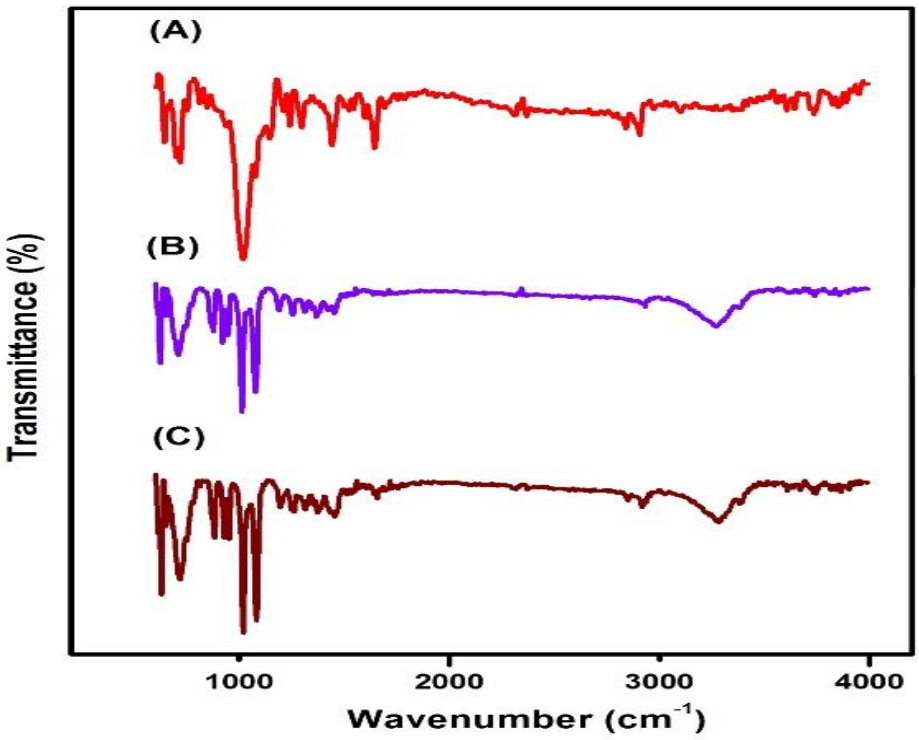


**Figure 8.4:** FT-IR spectra of HP-β-CD (A), $Ana_{C15:0}$ (B), and $Ana_{C15:0}$-Nanosponge (C)

### *8.3.5 X-ray diffraction (XRD) study*

XRD analysis is prominently used as a tool to study cyclodextrins and their complexation with various compounds in powder form (Pawar and Shende 2020). Interaction between components in the formation of the nanosponge complex can be assessed by comparing XRD patterns of individual compounds and nanosponge. The appearance of new

diffraction peaks, as well as the shift of drug peaks or variations in their relative intensities, are the indications to confirm the formation of the nanosponge complex. The XRD patterns of $Ana_{C15:0,}$ HP-β-CD, and nanosponge were shown in Figure 8.5. Evidence of several peaks was observed in the XRD pattern of $Ana_{C15:0}$ (Figure 8.5) at diffraction angles (2θ) 9.02, 13.4, 17.9, 20.2, and 22.8, indicating crystallinity while XRD patterns of HP-β-CD did not show the presence of sharp peaks suggesting amorphous nature. Further, the complete absence of $Ana_{C15:0}$ peaks was observed in the XRD patterns of nanosponge, suggesting the formation of a complex consisting of solid phase and also transition from crystalline to amorphous form.

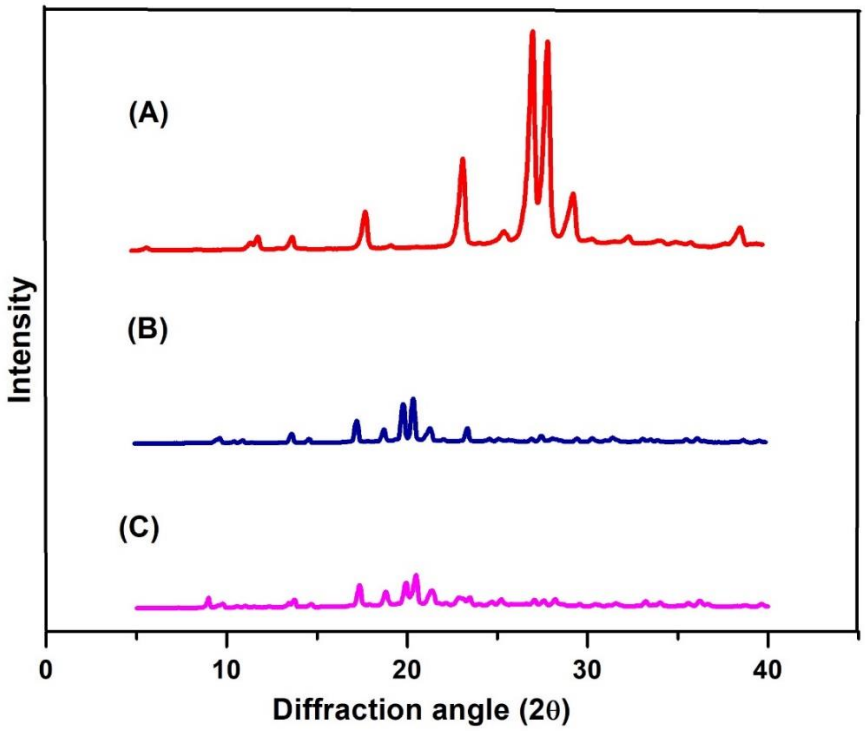


**Figure 8.5:** XRD spectra of HP-β-CD (A), $Ana_{C15:0}$ (B) and $Ana_{C15:0}$-Nanosponge (C).

### *8.3.6 Morphology evaluation of $Ana_{C15:0}$ encapsulated nanosponge*

The TEM image of $Ana_{C15:0}$-NS is illustrated in Figure 8.6. $Ana_{C15:0}$-NS appeared spherical in shape with uniform particle distribution. The size of the particles was in agreement with the particle size obtained via the DLS study.

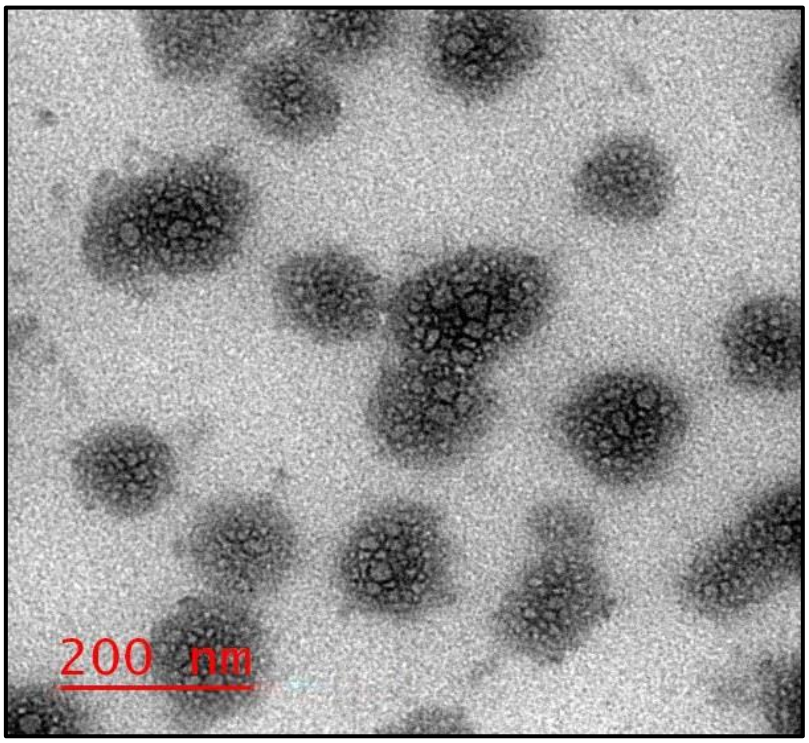


**Figure 8.6:** Photograph showing a TEM image of $Ana_{C15:0}$-NS

### *8.3.7 In-vitro release study*

*In-vitro* release profiles of $Ana_{C15:0}$-suspension and $Ana_{C15:0}$-NS is depicted in Figure 8.7. Both $Ana_{C15:0}$ and $Ana_{C15:0}$-NS exhibited initial burst release during the first one hour, i.e., 54.18±4.97% and 32.30±1.01% of $Ana_{C15:0}$ were released, respectively. Moreover, $Ana_{C15:0}$-NS demonstrated biphasic drug release patterns, i.e., initial burst release followed by sustained release. The release kinetics data suggested the Higuchi release kinetics as the $R^2$ value ($R^2$= 0.9641) was maximum.

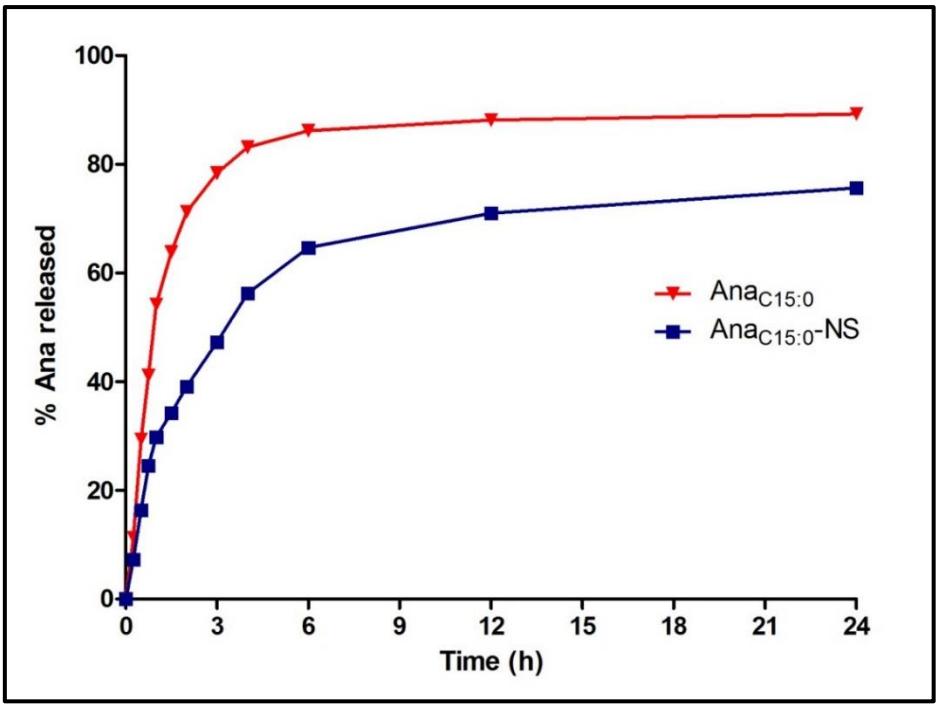


**Figure 8.7:** *In-vitro* drug release profiles of Ana$_{C15:0}$ and Ana$_{C15:0}$-NS. Graph represents the cumulative amount of Ana$_{C15:0}$ with respect to time

### *8.3.8 Evaluation of Ana$_{C15:0}$-NS topical gel*

#### *8.3.8.1 Texture profile analysis*

The mechanical properties of Ana$_{C15:0}$-NS hydrogel, like hardness, adhesiveness, and elasticity, have been depicted in Table 8.5. The properties of the hydrogel depend on the 3D architecture of the gel obtained due to the swelling property of the polymer used (Gade, Patel et al. 2019). These mechanical properties were derived from the TPA graph obtained between force (g) and time (s). The results indicate that the properties of the gel remain unchanged upon the addition of Ana$_{C15:0}$-NS in the gel base. This may be attributed to the smaller size of the nanosponge and incorporation of Ana$_{C15:0}$-NS into the 3D matrix of the hydrogel.

**Table 8.5:** Changes in mechanical properties of hydrogel upon the incorporation of $Ana_{C15:0}$-NS

| **Hydrogel properties** | **Blank gel** | **Ana-gel** | **Ana-NS gel** |
|---|---|---|---|
| Hardness (*N*) | 7.2±0.6 | 7.3±1.1 | 7.4±1.2 |
| Adhesiveness (*N*-mm) | 34.2±2.7 | 35.9±2.7 | 36.8±3.1 |
| Elasticity (mm) | 4.8±0.6 | 4.7±0.5 | 4.48±0.5 |

### *8.3.8.2 Ex-Vivo skin permeation and retention study*

To assess the influence of the $Ana_{C15:0}$ encapsulated nanosponge on the permeation and accumulation of drug into the skin, *ex vivo* skin permeation and retention studies were performed using rat skin employing Franz diffusion cells. After application of nanosponge gel, a greater quantity of drugs remained localized in the skin, with lesser amounts penetrating into the receptor compartment. $Ana_{C15:0}$-NS gel had the highest uptake of $Ana_{C15:0}$ in skin when compared with conventional $Ana_{C15:0}$ gel therefore the drug localization effect in the skin seems possible with use of NS (Figure 8.8 A). The cumulative amounts of $Ana_{C15:0}$ permeated through the skin from the conventional gel ($Ana_{C15:0}$-gel) and $Ana_{C15:0}$-NS gel at 24 h were 9.89±1.43 µg/cm$^2$ and 19.95±2.65 µg/cm$^2$, respectively. In other words, conventional gel showed lower drug permeation in comparison to nanosponge (Figure 8.8 B). $Ana_{C15:0}$-NS gel showed significant drug retention in the skin as compared to conventional $Ana_{C15:0}$-gel as drug retained in the skin was approximately 22.78±2.34% after 24 h in conventional $Ana_{C15:0}$-gel, while it was 43.81±4.36% after 24 h in case of $Ana_{C15:0}$-NS gel. Nanosponges have been reported earlier for enhancement of skin penetration (dermal delivery), especially into the upper skin layers, thereby have the potential of creating a reservoir that can prolong the skin residence time (Argenziano, Haimhoffer et al. 2019). The increased skin delivery by nanosponge results due to large particle surface area and small particle sizes.

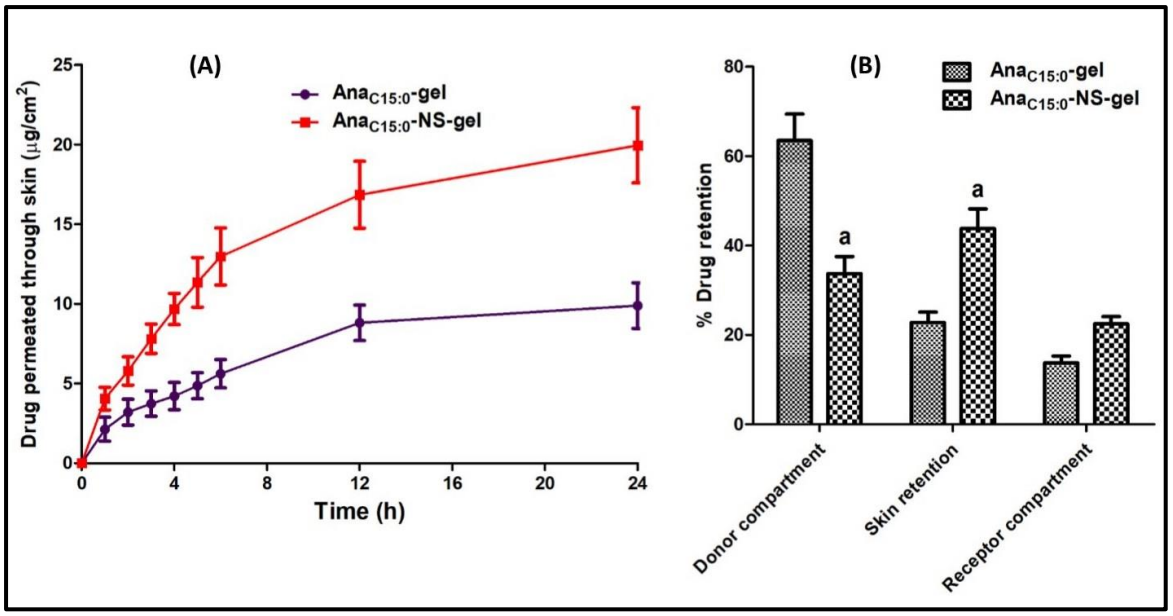


**Figure 8.8:** (A) Cumulative amount of drug permeated through skin with respect to time from Ana$_{C15:0}$-gel and Ana$_{C15:0}$-NS-gel. (B) Percentage drug retained in different compartments from Ana$_{C15:0}$-gel and Ana$_{C15:0}$-NS-gel. All data are presented as mean±SD (n=3) [a]represents significant difference compared to Ana$_{C15:0}$-gel, P<0.001 two-way ANOVA followed by Bonferroni posttest.

### *8.3.9 Physical evaluation of skin photoaging*

At the end of the experiment, the severity of skin damage was assessed by visual observation. Different groups receiving UV-B radiation and treatments are shown in Figure 8.9. Maximum damage (sunburn) characterized by skin lesions and large wrinkles could be witnessed in the UV-B irradiated group while the normal control group without UV-B irradiation did not reveal any lesions on the skin, indicating the fact that lesions caused due to UV-B irradiation. The treatment groups revealed remarkable healing potential, and the maximum healing was observed with the Ana$_{C15:0}$-NS-gel treatment (group V).

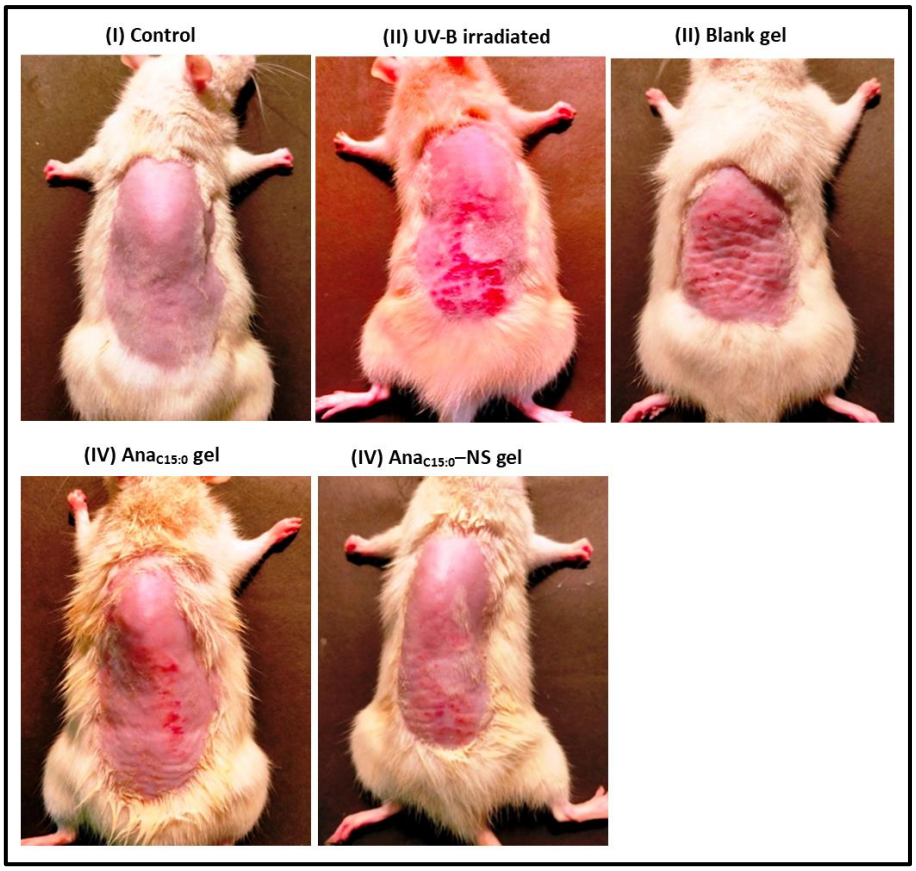


**Figure 8.9**: Photographs indicating the effect of UV-B radiation on the animals in different treatment groups. There was no visible lesion or redness in the control group (I), severe photoaging could be observed in the UV-B irradiated group (II), whereas the severity decreases on treatment with Ana$_{C15:0}$-gel (IV) and Ana$_{C15:0}$-NS gel (v)

### *8.3.10 Histopathology study*

The microscopic evaluation of the dorsal skin collected from rats is demonstrated in Figure 8.10. A significant increase in skin inflammatory disorder characterized by enhanced epidermal thickness was prominent in the UV-B irradiated group (Figure 8.10 b); closer examination revealed evidence of an abnormal increase in the epidermal cell number (hyperplasia) cell size (hypertrophy), and thickness of the stratum granulosum (hypergranulosis). However, the control group (Figure 8.10 a) not receiving any radiation demonstrated lesser epidermal thickness indicating the absence of inflammatory symptoms. The inflammatory skin symptoms were lesser visible in the case of Ana$_{C15:0}$

gel treated rats (Figure 8.10 c), while the highest healing was evident in the $Ana_{C15:0}$-NS gel treated group (Figure 8.10 d). The results were further correlated with the biochemical estimation parameters, and it was concluded the data obtained were in line with the hypothesis.

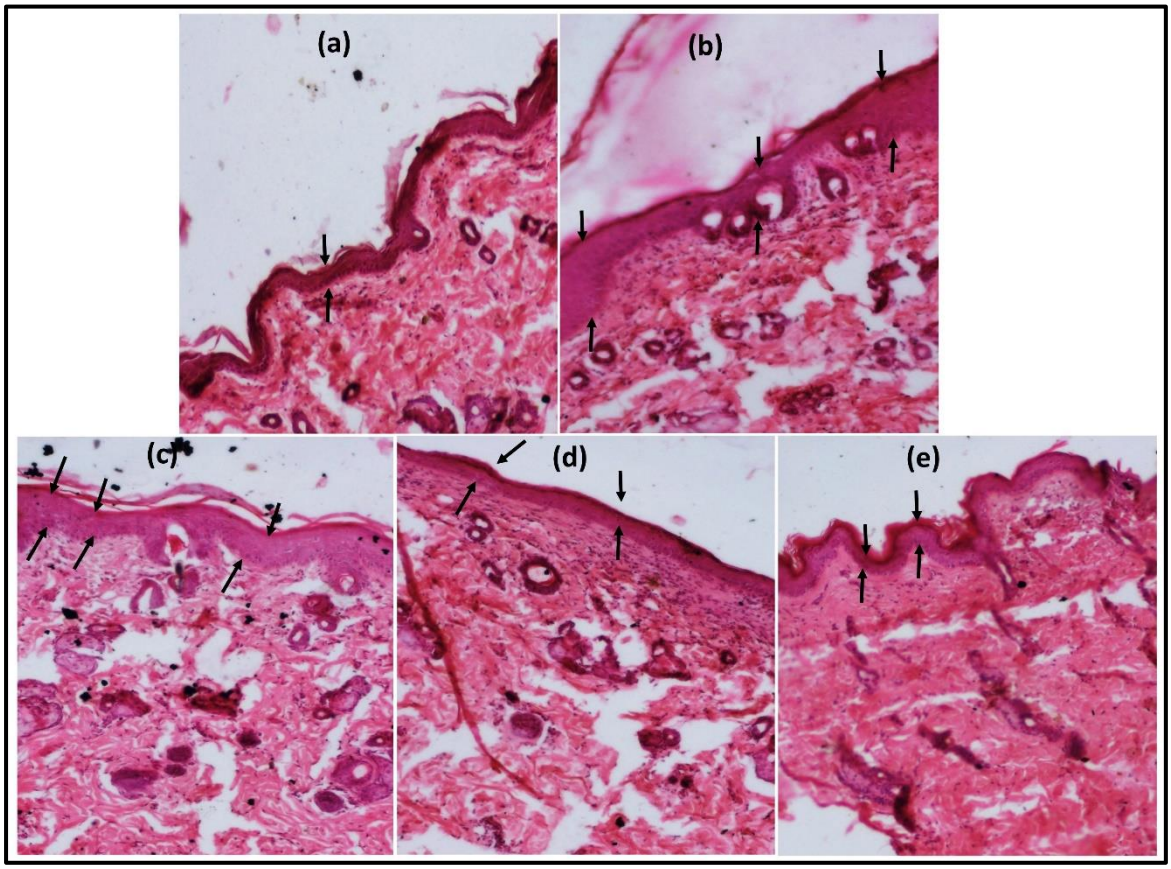


**Figure 8.10:** Histological examination of the H&E stained dorsal skin samples taken from different groups; control (a), UVB-irradiated (b), Blank gel treated (c), 0.1% $Ana_{C15:0}$-gel treated, and 0.1% $Ana_{C15:0}$-NS gel treated group.

### *8.3.11 Estimation of biochemical parameters*

#### *8.3.11.1 Determination of reactive oxygen species (ROS) level*

Skin is the most sensitive organ to UV radiation, which leads to increased ROS generation and causes skin photoaging. ROS in addition to damaging lipids, DNA, RNA proteins, and mitochondria; alters the structure, components, and functions of ECM such as collagen, elastin, gelatin, glycosaminoglycans, and fibroblasts. Production of ROS

leads to structural and functional alterations of the ECM and also causes direct detrimental chemical alterations to cellular components (Hwang, Park et al. 2014). Moreover, ROS activates cell surface cytokines and induces expression of transcription factor AP-1, ultimately stimulating expression of MMPs. Role of MMPs has already been established in damaging the ECM of the skin (Herrling, Jung et al. 2006). Therefore, a compound like Anacardic Acid having an additional antioxidant effect can be pathbreaking in the therapy of skin damage. Figure 8.11 demonstrates relative ROS production by different treatment groups considering ROS produced by UV-B irradiated group be 100%. It is clear from the graph that the formulation ($Ana_{C15:0}$-NS gel) significantly ($p<0.05$) reduces ROS production. Furthermore, nanosponge formulation delivered extraordinary potential to $Ana_{C15:0}$ in enhancing its ROS scavenging potential. Thus, $Ana_{C15:0}$ encapsulated nanosponge can be considered as a potential therapeutic alternative for ROS reduction as anticipated in the hypothesis.

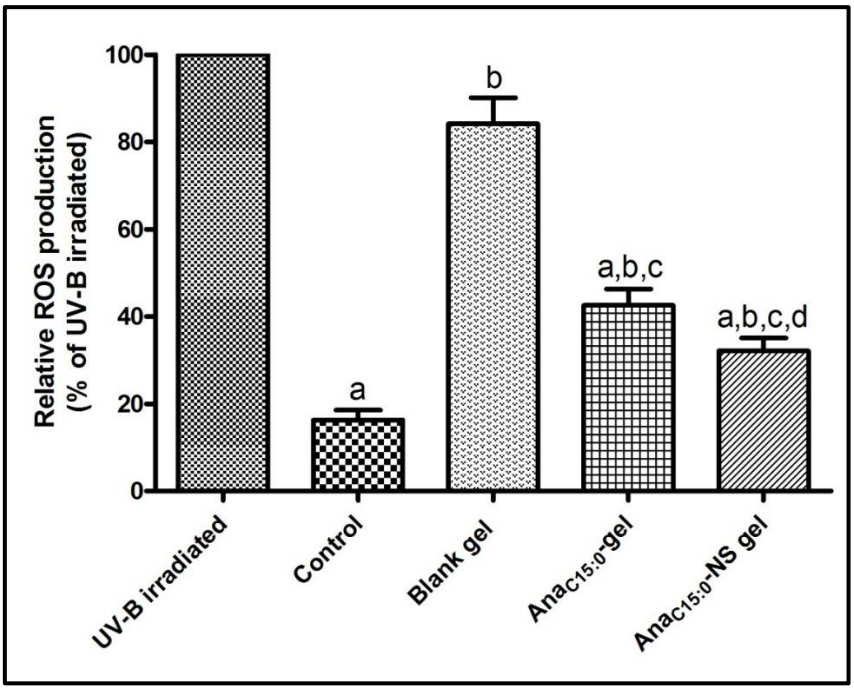


**Figure 8.11:** Effect of different treatment groups on ROS production. All data are presented as mean±SD (n=3) [a]represents significant difference as compared to UV-B

irradiated group [b] represents significant difference compared to control [c]represents significant difference compared to Blank gel [d]represents significant difference compared to $Ana_{C15:0}$-gel. $p<0.005$ one-way ANOVA followed by Newman-Keuls multiple-comparison test.

#### *8.3.11.2 Western blot study*

Exposure to UV radiation, especially UV-B radiation, leads to upregulation of MMP-1 and HAT P300 enzymes, ultimately resulting in skin photoaging. Exposure to UV-B radiation resulted in significantly higher expression levels of MMP-1 and HAT P300 enzymes (UV-B treated group). However, $Ana_{C15:0}$ gel treatment showed a remarkable reduction in the expression of those enzymes. Moreover, the treatment involving $Ana_{C15:0}$-NS gel resulted in a significant ($p<0.005$) reduction in the expression of MMP-1 and HAT P300, indicating the healing potential of $Ana_{C15:0}$-NS gel (Figure 8.12). The data in Figure 8.12 represents the relative levels of MMP-1 and HAT P300, which confirms the fact that the expression of enzymes involved in photoaging has been remarkably reduced upon treatment with $Ana_{C15:0}$-NS gel. UV-B radiation is a potent physical causative agent for skin photoaging, causes skin damage by up-regulation of HAT P300 and MMP-1 expression, which in turn lead to downregulation of skin collagen formation and causes damage to dermal fibroblasts, thus play a crucial role in the development of skin wrinkles and other skin aging symptoms (Cavinato and Jansen-Dürr 2017). Therefore, we evaluated the effect of $Ana_{C15:0}$ encapsulated nanosponge gels on the expression of HAT P300 and MMP-1, and the findings, as stated earlier, were found to be in accordance with our proposed hypothesis. Findings of the study was also supported by a similar study by Cho et al. 2017, in which the effect of *Coffea arabica* isolates was examined against UV-B induced skin fibroblast damage; they reported that the *Coffea arabica* isolates exhibit a potent effect on down-regulation of MMP-1, MMP-3, and MMP-9 (Cho, Bahuguna et al. 2017).

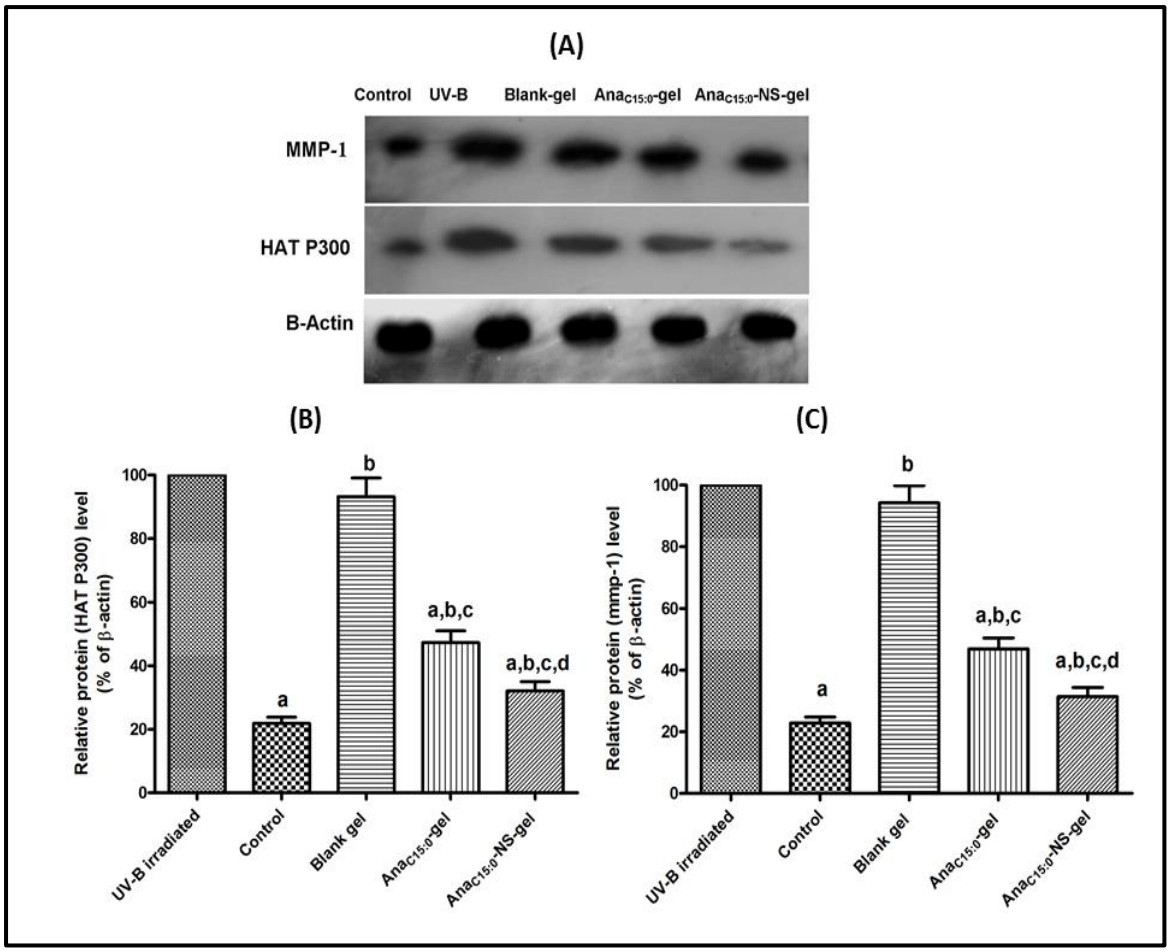


**Figure 8.12:** Effect of different treatment groups on the expression of MMP-1 & HAT p300 enzymes (A), relative level of HAT P300 among various groups (B), and relative MMP-1 level in different groups under study. All data are presented as mean±SD (n=6) **[a]** represents significant difference as compared to UV-B irradiated group **[b]**represents significant difference as compared to control, **[c]**represents significant difference as compared to Blank gel **[d]**represents significant difference as compared to Ana$_{C15:0}$-gel $p<0.005$ one-way ANOVA followed by Newman-Keuls multiple-comparison test.